Phonon dynamics and inelastic neutron scattering of sodium niobate

S. K. Mishra,[1,*] M. K. Gupta,[1] R. Mittal,[1] M. Zbiri,[2] S. Rols,[2] H. Schober,[2] and S. L. Chaplot[1]

[1]*Solid State Physics Division, Bhabha Atomic Research Centre, Trombay, Mumbai-400085, India*

[2]*Institut Laue-Langevin, BP 156, 38042 Grenoble Cedex 9, France*

(Received 13 December 2013; revised manuscript received 22 April 2014; published 16 May 2014)

Sodium niobate ($NaNbO_3$) exhibits an extremely complex sequence of structural phase transitions in the perovskite family and therefore provides an excellent model system for understanding the mechanism of structural phase transitions. We report temperature dependence of inelastic neutron scattering measurements of phonon densities of states in sodium niobate. The measurements are carried out in various crystallographic phases of this material at various temperatures from 300 to 1048 K. The phonon spectra exhibit peaks centered on 19, 37, 51, 70, and 105 meV. Interestingly, the peak near 70 meV shifts significantly towards lower energy with increasing temperature, while the other peaks do not exhibit any appreciable shift. The phonon spectra at 783 K show prominent change and become more diffusive as compared to those at 303 K. In order to better analyze these features, we have performed first-principles lattice dynamics calculations based on the density functional theory. The computed phonon density of states is found to be in good agreement with the experimental data. Based on our calculation we are able to assign the characteristic Raman modes in the antiferroelectric phase, which are due to the folding of the T ($\omega = 95$ cm^{-1}) and Δ ($\omega = 129$ cm^{-1}) points of the cubic Brillouin zone, to the A_{1g} symmetry.

DOI: 10.1103/PhysRevB.89.184303 PACS number(s): 78.70.Nx, 63.20.−e, 63.20.dk

I. INTRODUCTION

Materials exhibiting ferroelectric/piezoelectric properties are a subject of keen interest due to their potentially practical applications ranging from high density memories to advanced robotic technology (as sensor and actuator) [1–4]. Niobate based materials are environment friendly and appropriate for wide piezoelectric applications due to their piezoresponse that is comparable to Pb(Zr Ti)O_3. One of the end members, $NaNbO_3$, is a well-documented antiferroelectric that also finds applications in high density optical storage, enhancement of nonlinear optical properties, as hologram recording materials, etc. [3–5]. Relaxor type behavior in $NaNbO_3$ based solid solutions has also been reported [5].

Beyond the technological application, $NaNbO_3$ has been a rich model system for understanding of the mechanism of structural phase transitions. This system exhibits one of the most complex sequences of structural phase transitions in the perovskite family [6,7]. Above 913 K it has a paraelectric cubic phase ($Pm3m$). On lowering the temperature it undergoes transition to a series of antiferrodistortive phases in this order: tetragonal ($T2$) $P4/mbm$, orthorhombic ($T1$) $Cmcm$, orthorhombic (S) $Pbnm$, orthorhombic (R) $Pbnm$, orthorhombic (P) $Pbcm$ phases, and a rhombohedral $R3c$ phase. In a previous work we have carried out detailed neutron diffraction study in the temperature range 17 to 350 K [6]. We unambiguously provided [6] experimental evidence for the coexistence of the ferroelectric (FE) $R3c$ phase and the antiferroelectric (AFE) phase ($Pbcm$) over a wide range of temperatures. This phase coexistence and the reported anomalous dielectric response are consistent with competing ferroelectric and antiferroelectric interactions. Recent high pressure neutron diffraction measurements carried out up to 11 GPa at ambient temperature indicate transition from the $Pbcm$ to the $Pbnm$ phase [8]. These transitions are characterized by the appearance and disappearance of superlattice reflections in the powder diffraction patterns. The superlattice reflections originate from the condensation of zone-center and zone-boundary phonon modes. Thus, the stability of various crystallographic phases could be understood in terms of phonon instabilities.

The materials with perovskite structure have been a subject of intense numerical investigations by means of first-principles calculations [9–13]. The focus is on the ground-state structure and properties, lattice dynamics, and dielectric and piezoelectric response functions. Virtually all perovskites exhibit high-symmetry (cubic) structure at high temperatures. Phonons have been known to play a key role in the understanding of structural phase transitions in ferroelectrics. Most of the ferroelectric transitions are governed by softening of phonon modes in the high-symmetry phase. First-principles calculation is known to be a valuable tool to identify phonon frequencies and other related characteristics. The cubic perovskite structure has unstable modes and it is therefore subject to energy-lowering distortions like zone-center distortions (resulting in ferroelectricity) and zone-boundary distortions involving rotations and/or tilting of the oxygen octahedra.

Phonons can be probed via various experimental methods, including infrared absorption, and inelastic neutron and light scattering [14–17]. To understand the phase transition behavior of $NaNbO_3$, some studies of the temperature dependence of the Raman and infrared spectra [15–19] were performed. However, these measurements are limited to the Brillouin zone center and do not give a comprehensive picture of the dynamics. In this context, the combination of inelastic neutron scattering and first-principles calculations forms an adequate framework to obtain accurately phonon frequencies. Both the experimental and computational techniques are helpful to understand the role of structural distortions and their correlation to phonon instabilities, leading to phase transitions in this material.

*Corresponding author: skmsspd@barc.gov.in

Machado *et al*. [9] computationally investigated the relative phase stability of sodium niobate using LDA and GGA-WC (Wu and Cohen modified GGA) function. Additionally, they calculated full-phonon dispersion curves of the cubic structure to search for lattice instabilities in the whole Brillouin zone. They have reported indeed detailed description of the polar mode (responsible for ferroelectricity) and the rotational modes (R_{25} and M_3). On the other hand, the focus of our study is to correlate the specific phonon modes relevant to the observed structural distortions of the antiferroelectric phase. We have also calculated the phonon spectra of $NaNbO_3$ in the antiferroelectric orthorhombic (*Pbcm*), ferroelectric rhombohedral (*R*3*c*), and cubic (*Pm*3*m*) phases. We have successfully identified the characteristic antiferroelectric Raman modes, which are responsible for stabilization of the antiferroelectric phase. We established correlation between specific symmetry points in the cubic phase and the zone-center irreducible representations of the antiferroelectric orthorhombic phase. We have also succeeded in assigning the Raman and infrared modes, which are essential for the understanding of the nature of structural phase transitions induced by the change of the temperature, pressure, and composition. We also report results of inelastic neutron scattering measurements of phonon spectra in different crystallographic phases of sodium niobate from 300 to 1048 K. The results of inelastic neutron scattering experiment provide an opportunity to validate our calculations as well as important insights into the correlations between vibrational spectra and phase transitions. This paper is organized as follows: The details of the experimental technique and first-principles calculations are summarized in Secs. II and III, respectively. Section IV is dedicated to the presentation and discussion of the results. Conclusions are drawn in Sec. V.

II. EXPERIMENTAL DETAILS

The temperature dependent inelastic neutron scattering experiment on $NaNbO_3$ was carried out using the IN4C spectrometer at the Institut Laue Langevin (ILL), Grenbole, France. The spectrometer is based on the time-of-flight technique and is equipped with a large detector bank covering a wide range of about 10° to 110° of scattering angle. Polycrystalline sample of about 20 g of $NaNbO_3$ was placed in a thin cylindrical niobium container for neutron measurements. The measurements were done in the neutron-energy-gain mode using the incident neutron energy of 14.2 meV (2.4 Å). Several inelastic runs were recorded on the increase of temperature from 300 to 1048 K. In the incoherent one-phonon approximation, the phonon density of states [20] is related to the measured scattering function $S(Q,E)$, as observed in the neutron experiments by

$$g^{(n)}(E) = A\left\langle \frac{e^{2W_k(Q)}}{Q^2} \frac{E}{n(E,T)+\frac{1}{2}\pm\frac{1}{2}} S(Q,E)\right\rangle, \quad (1)$$

$$g^{n}(E) = B\sum_k \left\{\frac{4\pi b_k^2}{m_k}\right\} g_k(E), \quad (2)$$

where the + and − signs correspond to energy loss and gain of the neutrons, respectively, and $n(E,T) = [\exp(E/k_BT)-1]^{-1}$. A and B are normalization constants and b_k, M_k, and $g_k(E)$ are, respectively, the neutron scattering length, mass, and partial density of states of the kth atom in the unit cell. The quantity within angular brackets represents the average over all Q values. $2W_k(Q)$ is the Debye-Waller factor. The phonon density of states is corrected from multiphonon and Debye-Waller contributions in a self-consistent way according to the formalism developed by Sjolander [21] in the incoherent approximation [22]. The "MUPHOCOR" program, available as a routine in the ILL Lamp package, allows doing the calculations up to the fifth multiphonon term and was developed by Reichardt [23].

III. COMPUTATIONAL DETAILS

Relaxed geometries and total energies were obtained using the projector-augmented wave formalism [24] of the Kohn-Sham formulation of the density-functional theory [25] at the generalized gradient approximation (GGA) level, implemented in the Vienna *ab initio* simulation package (VASP) [26]. The GGA was formulated by the Perdew-Burke-Ernzerhof (PBE) density functional [27]. All results converge well with respect to k mesh and energy cutoff for the plane-wave expansion. An energy cutoff of 1100 eV and $8\times8\times8$ k-point mesh are found to be sufficient for an accuracy of 10^{-4} eV in total energy calculations. The k-point mesh has been generated using the Monkhorst-Pack (MP) scheme [28]. The electronic energy convergence criterion was set to 10^{-8} eV. Hellmann-Feynman forces following geometry optimization were less than 10^{-4} eV Å^{-1}. Full geometry optimization, including cell parameters, was carried out on $NaNbO_3$, in the antiferroelectric and ferroelectric phases. Neutron diffraction measurements showed that the two phases coexist over a wide temperature range (17–250 K) [6]. Table I compares the calculated and experimental structural parameters for both phases. The calculated lattice parameters are found to be slightly overestimated as compared to the experimental ones, as expected from GGA calculations.

At room temperature $NaNbO_3$ crystallizes in the orthorhombic phase (*Pbcm*) with 8 f.u. per unit cell (40 atoms). This leads to 120 phonon branches (3 acoustic modes + 117 optical modes). From the group theoretical analysis, the irreducible representations of the zone-center optical phonons are $\Gamma_{\text{optical}} = 15A_g + 17B_{1g} + 15B_{2g} + 13B_{3g} + 13A_u + 14B_{1u} + 16B_{2u} + 14B_{3u}$, where the A_g, B_{1g}, B_{2g}, and B_{3g} modes are Raman active, whereas the modes A_u are both Raman and infrared inactive. The modes B_{1u}, B_{2u}, and B_{3u} are infrared active. Hence, 60 Raman active modes are expected in the orthorhombic phase (*Pbcm*).

At low-temperature $NaNbO_3$ is rhombohedral (*R*3*c*) with 2 f.u. per unit cell (10 atoms), resulting in 30 phonon branches (3 acoustic modes +27 optical modes). The irreducible representations of the zone-center optical modes are $\Gamma_{\text{optical}} = 5A_1 + 4A_2 + 9E$. The A_1 and the doubly degenerate E modes are both Raman and infrared active, whereas the A_2 mode is both Raman and infrared inactive. Therefore, 23 Raman active phonons are expected in the rhombohedral phase (*R*3*c*).

In order to determine all force constants, the supercell approach was used for the lattice dynamics calculations. Total energies and Hellmann-Feynman forces were calculated for 42, 18, and 8 structures corresponding to the *Pbcm*, *R*3*c*, and *Pm*3*m* phases, respectively, and resulting from individual

TABLE I. Experimental [6] and *ab initio* calculated structural parameters of $NaNbO_3$ in the orthorhombic, antiferroelectric phase (*Pbcm*) and in the rhombohedral, ferroelectric phase (*R*3*c*). The structural information of ferroelectric (*R*3*c*) phase compared with the result obtained by Ref. [9] (second row) with the Wu and Cohen version of GGA.

	Orthorhombic antiferroelectric phase (*Pbcm*)					
	Experimental positional coordinates			Calculated positional coordinates		
Atoms	*x*	*y*	*z*	*x*	*y*	*z*
Na1	0.247	0.75	0.00	0.260	0.7500	0.000
Na2	0.227	0.789	0.25	0.259	0.796	0.250
Nb	0.242	0.282	0.131	0.243	0.279	0.125
O1	0.329	0.25	0.00	0.310	0.250	0.00
O2	0.208	0.278	0.25	0.191	0.227	0.25
O3	0.530	0.040	0.138	0.542	0.033	0.140
O4	0.975	0.489	0.107	0.960	0.456	0.110
	Lattice parameters (Å) $A_{orth} = 5.5012$ (Å); $B_{orth} = 5.5649$ (Å), $C_{orth} = 15.3972$ (Å)			Lattice parameters (Å) $A_{orth} = 5.568$ (Å); $B_{orth} = 5.645$ (Å), $C_{orth} = 15.603$ (Å)		
	Ferroelectric rhombohedral phase (*R3c*)					
	Experimental positional coordinates			Calculated positional coordinates		
Atoms	*x*	*y*	*z*	*x*	*y*	*z*
Na	0.272	0.272	0.272	0.273	0.273	0.273
				0.272[a]	0.272[a]	0.272[a]
Nb	0.016	0.016	0.016	0.014	0.014	0.014
				0.016[a]	0.016[a]	0.016[a]
O	0.320	0.183	0.747	0.312	0.184	0.749
				0.318[a]	0.191[a]	0.749[a]
	Lattice parameters (Å) $a_{rhom} = 5.552$ (Å), $\alpha = 59.16$ (deg)			Lattice parameters (Å) $a_{rhom} = 5.637$ (Å), $\alpha = 58.94$ (deg) $a_{rhom} = 5.570$ (Å), $\alpha = 59.15$ (deg)[a]		

[a]Reference 9.

displacements of the symmetry inequivalent atoms in the supercell, along the inequivalent Cartesian directions ($\pm x$, $\pm y$, $\pm z$). Phonon frequencies, Raman modes, and dispersion relations were extracted from subsequent calculations using the direct method [29] as implemented in the PHONON software [30].

A proper understanding of the functionality and phase transition behavior of the materials requires that the structural information as obtained from diffraction techniques should be adequately complemented by spectroscopic investigations like Raman and infrared spectroscopies. The mode assignments from Raman and infrared spectroscopies are essential to understand the nature of phase transition as a function of temperature, pressure, and composition. The assignment of phonon modes also helps to identify the atomic motions which drive the observed phase transition(s). The computed zone-center phonon frequencies for both the antiferroelectric and ferroelectric phases are shown in Fig. 1. As expected, the ferroelectric phase has less Raman modes than those found in the antiferroelectric phase.

IV. RESULTS AND DISCUSSION

Figure 2 depicts the evolution of inelastic neutron scattering (INS) spectra for NaNbO-$_3$ at $T = 303$, 783, 838, 898, and 1048 K. The spectra correspond to different crystallographic phases. Five features (broad peaks centered around 19, 37, 51, 70, and 105 meV) can be easily identified. At 303 K, additional well resolved peaks below 37 meV are also observed. Their intensity decreases significantly with increasing temperature. Remarkably, the peak around 70 meV shifts significantly

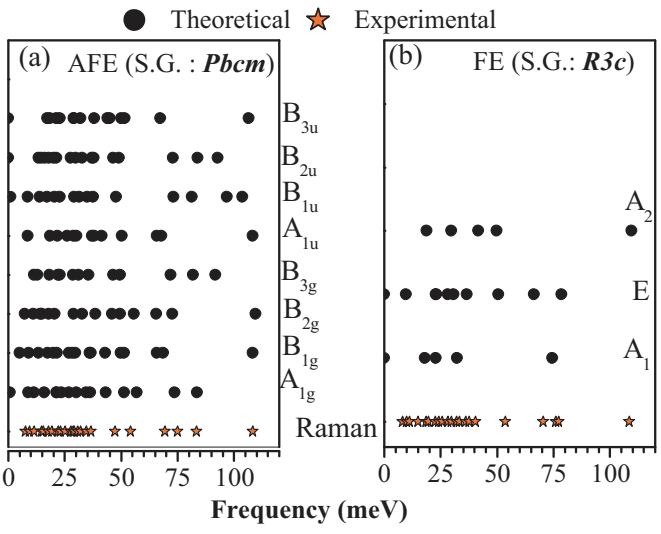

FIG. 1. (Color online) Comparison of the calculated (filled circles) long-wavelength phonon frequencies with the available experimental data (stars) [15–18] for both the antiferroelectric (AFE) and the ferroelectric (FE) phases.

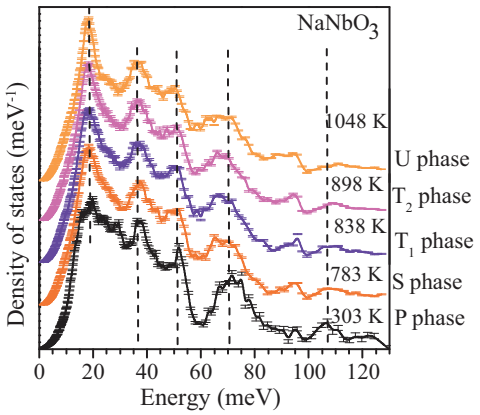

FIG. 2. (Color online) The temperature dependence of the phonon spectra of $NaNbO_3$ as observed by neutron inelastic scattering.

towards lower energies with increasing temperature, while the others do not change in a noticeable way. At 783 K, a prominent change is observed and the spectra become more diffusive than that at 303 K. The variation of the INS spectra is associated with the occurrence of phase transitions. Prominent changes in the phonon spectra are usually expected across strong first order phase transitions, while weak first or second order phase transitions lead to minimal changes. Upon heating, sodium niobate undergoes a strong first order phase transition at 680 K. On the other hand, all the other phase transitions above 783 K are of a weak first or second order in nature. Thus, a prominent change is only observed in the phonon spectra at 783 K, as compared to that at 303 K. Further heating above 783 K leads to phonon spectra resembling each other.

Figure 3 compares the experimental and calculated neutron-weighted phonon density of states of $NaNbO_3$, in the antiferroelectric phase. The calculations are found to be in fair agreement with the measurements. All the observed features are computationally well reproduced. Our *ab initio* lattice dynamics calculations show that both the ferroelectric ($R3c$) and the antiferroelectric ($Pbcm$) phases are dynamically stable (all frequencies are real). All the calculations were performed at zero temperature. The calculated free energies of ferroelectric (−7.8102 eV/atom) and antiferroelectric (−7.8082 eV/atom) phases are comparable. The small energy (∼2 meV/atom) difference between the two phases could explain the coexistence of both the phases observed in neutron powder diffraction experiments [6]. Machado *et al.* [9] have also computationally investigated the relative phase stability of sodium niobate and reported the similar behavior.

Recently, Jiang *et al.* [31] have performed refinements of neutron diffraction data to determine the local structure by the pair distribution function (PDF) method. They reported that the ground states of $NaNbO_3$ in the low-temperature antiferroelectric and ferroelectric phases have the $R3c$ symmetry, even though in the long range the system shows the $Pbcm$ symmetry or the coexistence of two phases. They argued that this structure tends to form nanotwins with irregular spacing, resulting in the appearance of a long-range antiferroelectric ($Pbcm$) phase. As mentioned earlier, the ferroelectric phase ($R3c$) phase has slightly lower energy in comparison to the antiferroelectric phase ($Pbcm$). This suggests that the ferroelectric phase is most likely and consistent with the results of Jiang *et al.* [31]. However, it is difficult to confirm the formation of nanotwins with irregular spacing using theoretical calculation. Due to its structural complexity, we have not modeled the twin structure.

The *ab initio* derived atomistic partial densities of states are shown in Fig. 4. The oxygen atoms contribute dynamically in the whole spectral range, up to 120 meV, while Nb atoms mainly contribute up to 75 meV. The vibrations due to the Na

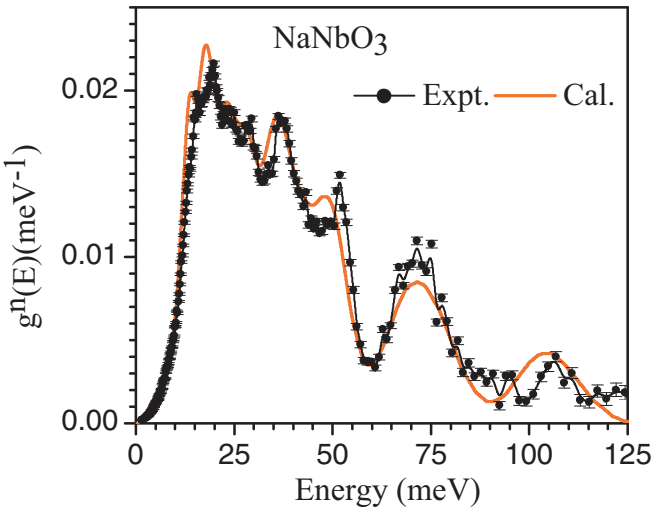

FIG. 3. (Color online) The experimental (dotted line at 303 K) and calculated (solid line at 0 K) phonon spectra for $NaNbO_3$ in the antiferroelectric phase ($Pbcm$). The calculated spectra have been convoluted with a Gaussian of FWHM of 15% of the energy transfer in order to describe the effect of energy resolution in the experiment.

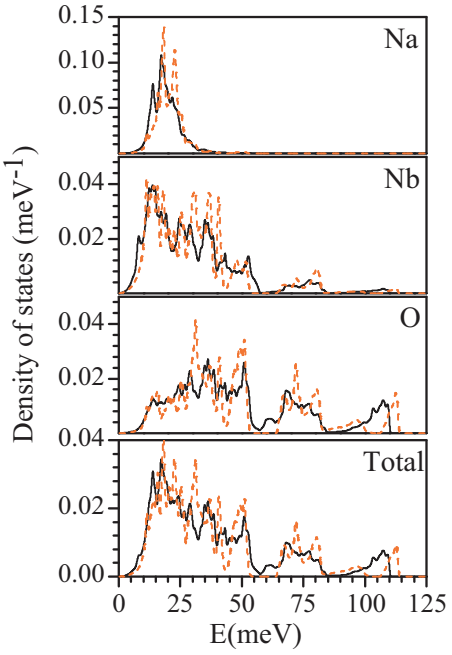

FIG. 4. (Color online) The calculated partial density of states for various atoms and the total phonon density of states for $NaNbO_3$, in both the antiferroelectric orthorhombic ($Pbcm$) phase (solid line) and the ferroelectric rhombohedral ($R3c$) phase (dashed line).

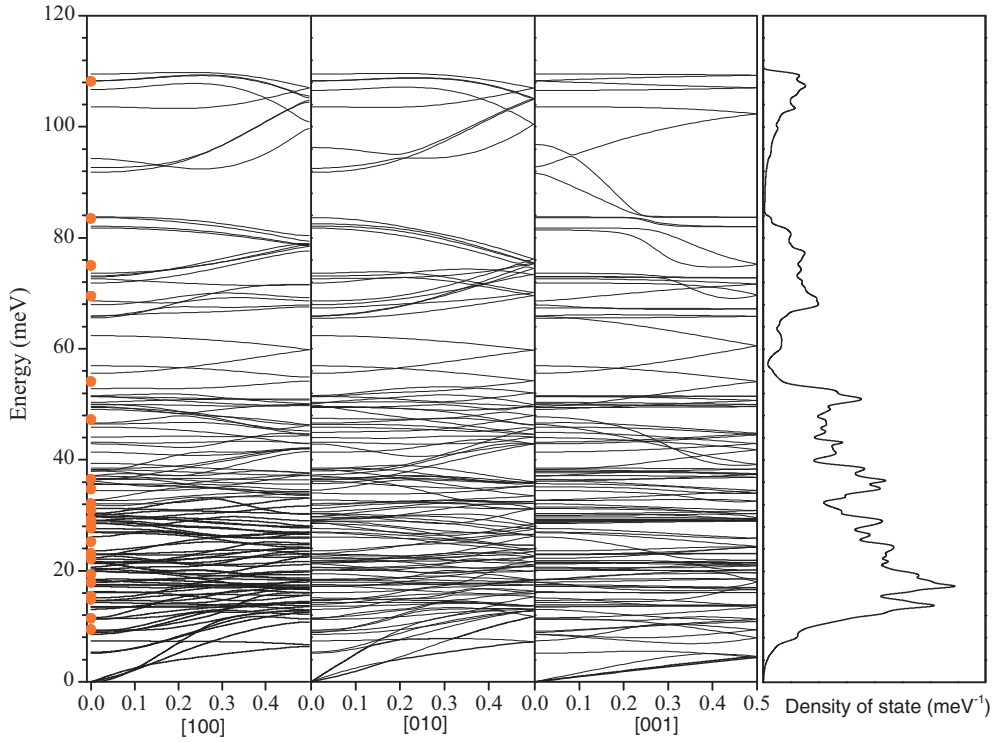

FIG. 5. (Color online) The calculated phonon dispersion relations for the orthorhombic phase (*Pbcm*) of $NaNbO_3$. For the sake of comparison, available experimental optical long wavelength data are also shown (solid circles) [15–18].

atom extend up to 40 meV. Computed partial density of state of Na reveals the presence of three peaks in the antiferroelectric phase and two peaks for the ferroelectric phase. It can also be seen that spread in the partial density of state associated with Na is more in the antiferroelectric phase as compared to the ferroelectric phase. It can be interpreted in terms of Na-O bond lengths. For the antiferroelectric phase, there are two types of sodium and four types of oxygen atoms, which result in significant variation in bond length (change in the force constant), and in turn result in more spread in the partial density of state. While in the ferroelectric phase we have only one type of Na and O atom. In the ferroelectric phase Na atoms are shifted from the center of the oxygen cage and results in two different Na-O bond lengths. Similar interpretation also holds for partial density of states of niobium and oxygen atoms. It should be noticed that shorter bond lengths in the ferroelectric phase (with respect to the antiferroelectric phase) results in the extending of the energy range of the total density of states. It is interesting to note that band gap in the phonon density of states for the ferroelectric phase is larger as compared to that in the antiferroelectric phase.

To understand the vibrational properties of sodium niobate using inelastic scattering techniques, various attempts have been taken [15–19]. However they were limited to the zone center only. To the best of our knowledge, there are no experimental or theoretical reports extending the work to the zone boundaries (phonon dispersion relations) for the antiferroelectric phase. This might be due to the experimental complexity associated with measuring the 120 modes. The synthesis of a suitable single domain crystal could add more difficulties as well. Presently we report our *ab initio* calculated phonon-dispersion relations (Fig. 5). These are plotted along the high-symmetry directions of the Brillouin zone. Figure 5 also contains available Raman data from the literature. Our calculations are in a good agreement with the available zone-center experimental data.

The structural phase transitions in perovskite-type materials (ABO_3) originate from the competing interactions between different phonon instabilities occurring in the cubic phase. These transitions belong generally to two classes: ferrodistortive (FD) and antiferrodistortive (AFD) [1,32]. The FD and AFD phase transitions are driven by zone-center ($q = 0$) and zone-boundary phonons ($q \neq 0$), respectively. Known examples of these transitions are the cubic to tetragonal phase transition in $BaTiO_3$ and $PbTiO_3$, for the ferrodistortive case, and in $SrTiO_3$ and $CaTiO_3$, for the antiferrodistortive case [1,32]. The evolution of these phase transitions depends on the condensation sequence of the soft modes M_3 and R_{25}. The zone boundary R_{25} mode is threefold degenerate and the M_3 mode is nondegenerate. The triply degenerate R_{25} soft mode is made up of three components corresponding to the rotational degrees of freedom of the BO_6 octahedra around the three separate [001] axes. If one of the components condenses at the transition point, the resulting structure would be tetragonal $I4/mcm$, and the coupled condensation of the three components would lead to a rhombohedral $R3c$ structure. However, when with successive phase transitions associated with both the M_3 and R_{25} soft modes, the sequence of the phase evolution depends in a complex way on the condensation sequence of the soft mode [1,32].

Recently, Izumi and co-workers performed a detailed inelastic neutron scattering study in the cubic phase of

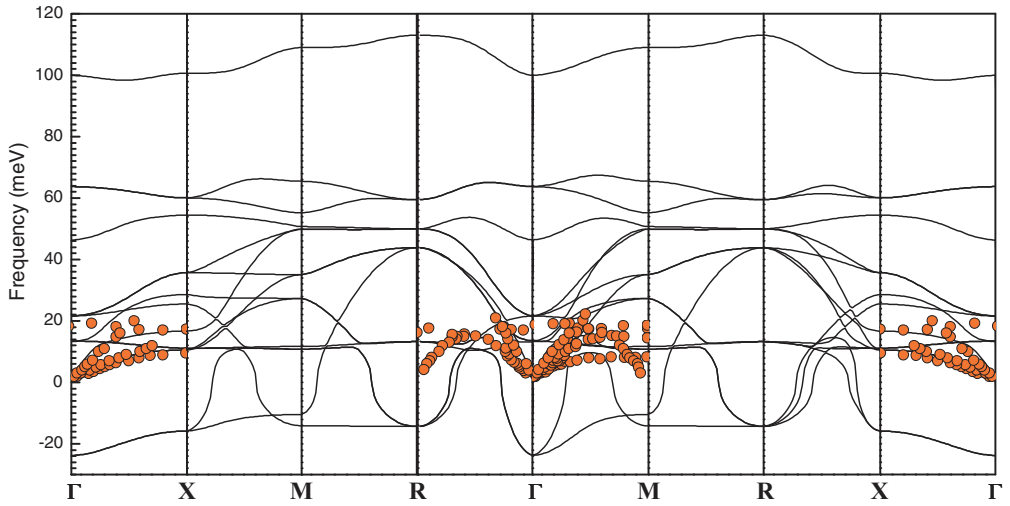

FIG. 6. (Color online) Computed phonon dispersion relations for cubic phase (*Pm3m)* of $NaNbO_3$ compared to reported experimental inelastic neutron scattering (INS) single crystal data (red circles) [14].

$NaNbO_3$ [14]. Their measurements show gradual softening of the transverse acoustic (TA) phonon modes at the zone boundary points *M* (½ ½ 0) and *R* (½ ½ ½). This indicates instabilities of the in-phase and out-of-phase rotations of the oxygen octahedra around the [001] direction. The softening of these modes suggests low-lying flat transverse acoustic dispersion relations along the zone-boundary line *M*-*R* (*T* line). As the temperature is decreased, these modes soften and become stable below the phase transition temperature. In order to detect these phonon instabilities using first-principles technique, we have calculated the phonon dispersions from the zone center (Γ) to the zone boundary points *R* and *M* (Fig. 6).

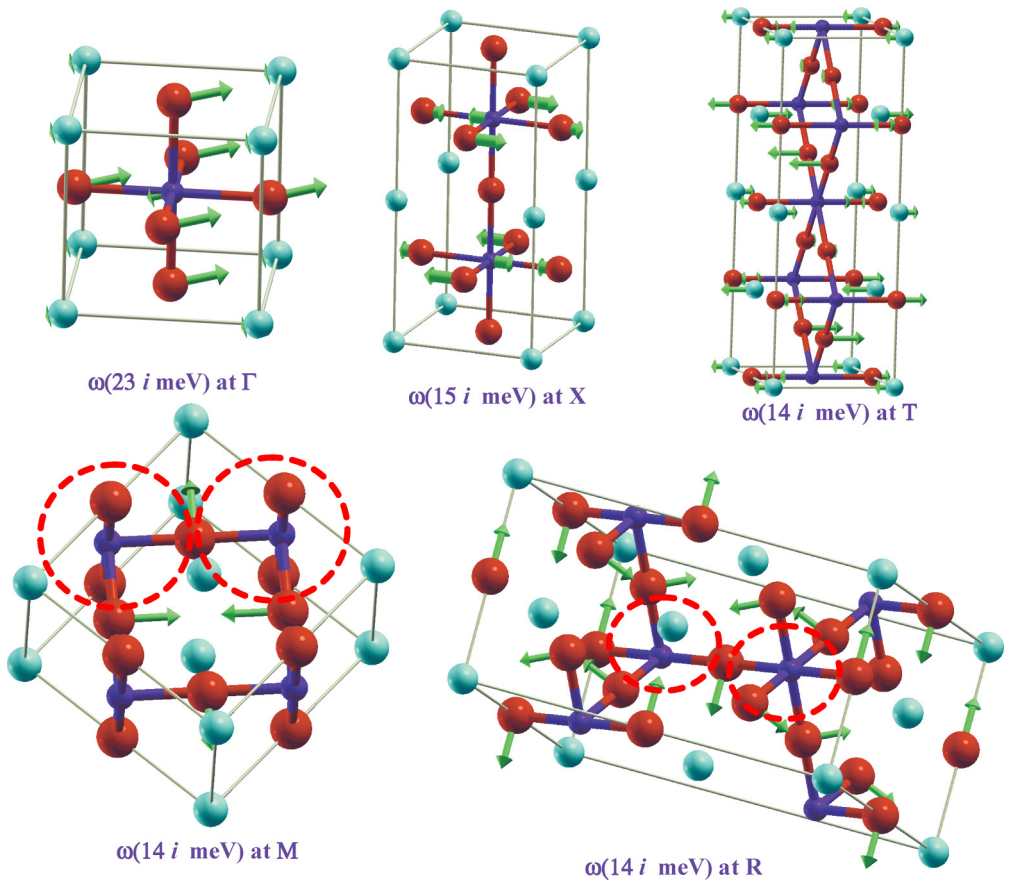

FIG. 7. (Color online) *Ab initio* derived eigenvectors of selected zone-center and zone-boundary unstable phonon modes at the Γ**,** *M*, *R*, *T*, and *X* points for the cubic phase of $NaNbO_3$. The lengths of arrows are related to the displacements of the atoms. Key: Na, cyan; Nb, blue; O, brown.

In general, we find a very good agreement between our calculations and Machado *et al.* [9], together with the experimental data from the literature [14]. Small deviations are expected as calculations were obtained at 0 K, whereas inelastic neutron scattering data were acquired in cubic phase (970 K).

From Fig. 6 one can see that, in contrast to $SrTiO_3$ [33], the polar instability strength at the Γ point is stronger than the antiferrodistortive instabilities at the R and M points, and it extends over a wider region of the Brillouin zone. Furthermore, the strength of the M and the R point instabilities are quite similar. Interestingly, the branches along the Γ-R and Γ-M directions show dramatic changes when reaching the R and M points. When moving away from M to R, two unstable modes are detected. One of them is rather flat and the other one shows rapid stiffening and becomes stable. Moreover, one of the stable modes become unstable at T (½ ½ ¼) point. Our results are consistent with other theoretical works in the literature [9].

Above 950 K, $NaNbO_3$ occurs in the cubic phase. On decreasing the temperature, it transforms to a tetragonal phase ($P4/mbm$). The first structural transformation is from cubic to tetragonal structure, where the unit cell is doubled in the plane perpendicular to the rotation axes of the M_3 mode. By further lowering the temperature, condensation of the R_{25} phonon leads to the orthorhombic $Cmcm$ (T_2) phase. Unstable phonon branches along the M-R line contribute to the occurring successive phase transitions. These phonons play an important role in stabilizing the different phases (P, S, and R) in $NaNbO_3$. In a previous study [7] we have proposed that the additional superlattice reflections are due to the condensation of the zone-boundary phonons at T ($q = ½, ½, g$). The orthorhombic structures of the S, R, and P phases result from the condensation of the phonon mode ($q = ½, ½, g$), with $g = 1/12$, $1/6$, and $1/4$. These orthorhombic phases originate from the modulation of the high-symmetry cubic phase, associated with the phonon modes at $q = (½, ½, g)$. Furthermore, the freezing of all the R_{25} modes and a zone-center phonon stabilizes the low-temperature ferroelectric rhombohedral phase. The detailed descriptions of the polar mode (responsible for ferroelectricity) and the rotational modes (R_{25} and M_3) are found to be similar to those reported by Machado *et al.* [9].

Deeper insights into phonon dynamics can be gained by performing an analysis of the eigenvectors corresponding to specific phonon modes, relevant to the present study. These are derived from our *ab initio* calculations and are plotted in Fig. 7. The eigenvector of the unstable Γ-point zone-center phonon mode at $\omega = 23i$ meV indicates clearly that niobium and oxygen atoms are moving in opposite directions. This leads to the formation of a dipole, and induces ferroelectricity. The eigenvectors corresponding to the unstable modes at M and R points ($\omega = 14i$ meV) exhibit an in-phase and out-of-phase rotation of the oxygen octahedra, leading to a doubling of the unit cell. The analysis of the eigenvector of the X-point zone boundary mode at $\omega = 15i$ meV suggests that, similar to the zone-center mode, Nb and O atoms move in opposite directions within a layer of the basal plan, and this motion is antiphased in an adjacent layer. This results in a zero total dipole moment in the unit cell. The displacement patterns are therefore related to antiferroelectricity. The mode at the T point having the phonon frequency $\omega = 14i$ meV possesses an eigenvector displacement indicating a multiplication of the unit cell.

TABLE II. Correlation diagram between specific symmetry points in the cubic phase and the zone-center irreducible representations of the antiferroelectric, orthorhombic phase.

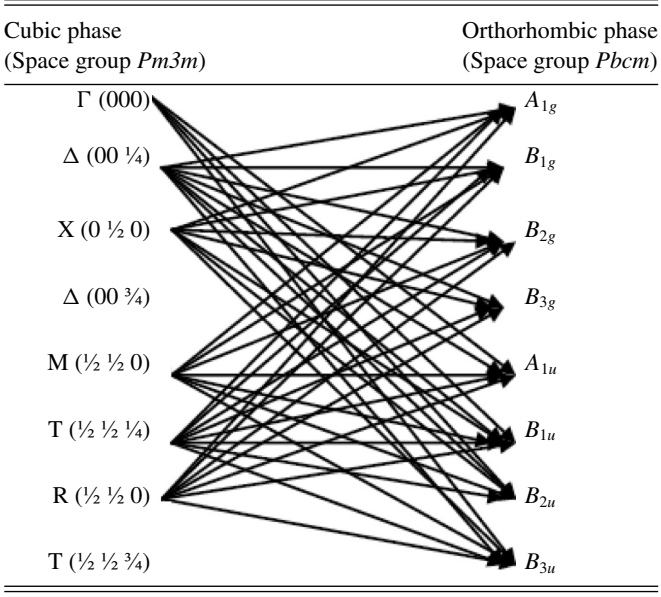

Before we close, we would like to identify the phonons which are responsible for the stabilization of the antiferroelectric phase. The antiferroelectric phase is found to accompany superlattice reflections in powder neutron diffraction data [6,7]. This is confirmed by the appearance of Raman lines in Raman spectroscopy. These lines become active due to the folding of the corresponding specific zone-center points, below the antiferroelectric phase transition temperature. To investigate these special points, we have established a symmetry-based correlation between the orthorhombic zone-center points and the high-symmetry points in the cubic phase (Table II). Below the antiferroelectric phase transition, strong modifications of the Raman scattering patterns are observed [15–19] accompanying the appearance of Raman modes around 93 and 123 cm^{-1}. Furthermore, a sudden enhancement of the intensity of the bands within the two frequency ranges 150–300 cm^{-1} and 500–650 cm^{-1} are also noted [15–19]. We have assigned the two lines at 93 and 123 cm^{-1} as belonging to the A_{1g} irreducible representation, and we have identified them as originating from the folding of the T (93 cm^{-1}) and Δ (129 cm^{-1}) points of the Brillouin zone under the cubic phase. The eigenvectors corresponding to the two AFE modes of $NaNbO_3$, as extracted from our *ab initio* lattice dynamical calculations, are shown in Fig. 8. The mode at 93 cm^{-1} involves significant motions of Na, Nb, and O, which are located at the sites 4d ($¼ + u, ¾ + v, ¼$), 8e ($¼ + u, ¼ + v, 1/8 + w$), and ($½ + u, 0 + v, 1/8 + w$), respectively. However, the Raman mode at 129 cm^{-1} reflects a significant displacement of all the atoms.

V. SUMMARY

We have reported inelastic neutron scattering measurements of the phonon density of states of sodium niobate as a function

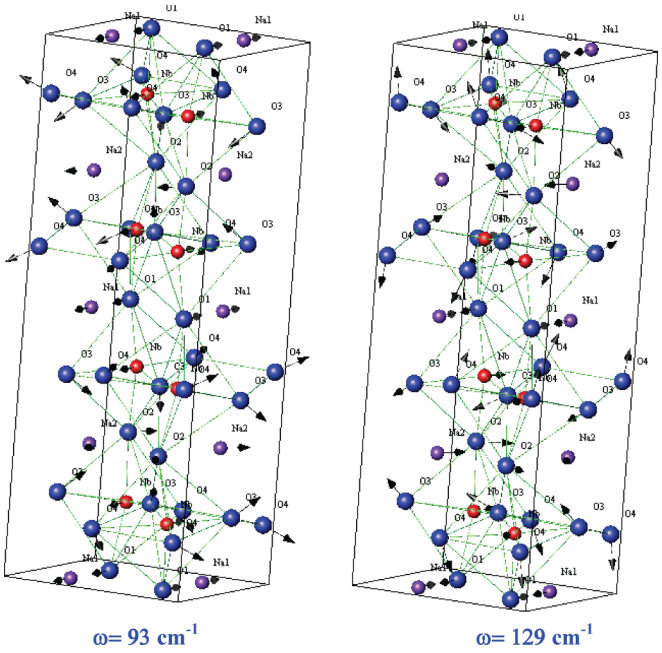

FIG. 8. (Color online) The eigenvectors of the two antiferroelectric modes at (a) $\omega = 93$ cm^{-1} and (b) 129 cm^{-1} of $NaNbO_3$, induced by the folding of the T (q = ½ ½ ¼) and Δ (q = 0 0 ¼) points of the Brillouin zone under the cubic phase, respectively. The lengths of the arrows are related to the displacements of the atoms. Key: Na: violet spheres; Nb: blue spheres; O: brown spheres.

of temperature. The inelastic neutron scattering spectra are correlated to the various crystallographic phases of $NaNbO_3$, and show significant changes with increasing temperature. The peak at 70 meV is found to shift to lower energies, while the other pronounced peaks are not noticeably affected. Upon heating, the spectra become more diffusive. In order to get deeper insights into the observed features, we have performed *ab initio* lattice dynamics calculations. The computed phonon density of states of $NaNbO_3$ is found to be in good agreement with our INS measurements. The calculated partial densities of states reveal that the dynamical contribution of the oxygen atoms spreads over the whole energy range, while the Nb atoms contribute mainly up to 75 meV. The vibrations due to Na atoms extend up to 30 meV. Above 75 meV, the dynamics is mainly due to the Nb-O stretching modes. Using the calculations, we have identified the various soft phonon modes at specific points in the Brillouin zone that are associated with various phase transition as a function of temperature. Furthermore, we have found that the characteristic antiferroelectric Raman modes, which appear below the antiferroelectric phase transition temperature, correspond to the A_{1g} symmetry and are due to the folding of the T ($\omega = 95$ cm^{-1}) and Δ ($\omega = 129$ cm^{-1}) points of the Brillouin zone, under the cubic phase.

ACKNOWLEDGMENTS

We would like to thank Mrs. P. Goel, Solid State Physics Division, Bhabha Atomic Research Centre, Mumbai, India for her cooperation during inelastic neutron measurements at ILL.

[1] M. E. Lines and A. M. Glass, *Principles and Application of Ferroelectrics and Related Materials* (Clarendon, Oxford, 1977); Xu. Yuhuan, *Ferroelectric Materials and Their Applications* (North-Holland Elsevier Science, Amsterdam, 1991); L. G. Tejuca and J. L. G. Fierro, *Properties and Applications of Perovskite-Type Oxides* (Dekker, New York, 1993).

[2] E. Bousquet, M. Dawber, N. Stucki, C. Lichtensteiger, P. Hermet, S. Gariglio, J. M. Triscone, and P. Ghosez, Nature (London) **452**, 732 (2008); T. Choi, Y. Horibe, H. T. Yi, Y. J. Choi, Weida Wu, and S.-W. Cheong, Nat. Mater. **9**, 253 (2010).

[3] Y. Saito, H. Takao, T. Tani, T. Nonoyama, K. Takatori, T. Homma, T. Nagaya, and M. Nakamura, Nature (London) **432**, 84 (2004); E. Cross, *ibid.* **432**, 24 (2004).

[4] E. Valdez, C. B. de Araujo, and A. A. Lipovskii, Appl. Phys. Lett. **89**, 031901 (2006); E. Hollenstein, M. Davis, D. Damjanovic, and Nava Setter, *ibid.* **87**, 182905 (2006); Yu. I. Yuzyuk, P. Simon, E. Gagarina, L. Hennet, D. Thiaudiere, V. I. Torgashev, S. I. Raevskya, I. P. Raevskii, L. A. Reznitchenko, and J. L. Sauvajol, J. Phys.: Condens. Matter **17**, 4977 (2005).

[5] P. Raevski, S. I. Raevskaya, S. A. Prosandeev, V. A. Shuvaeva, A. M. Glazer, and M. S. Prosandeeva, J. Phys.: Condens. Matter **16**, L221 (2004).

[6] S. K. Mishra, N. Choudhury, S. L. Chaplot, P. S. R. Krishna, and R. Mittal, Phys. Rev. B **76**, 024110 (2007), and reference therein.

[7] S. K. Mishra, R. Mittal, V. Y. Pomjakushin, and S. L. Chaplot, Phys. Rev. B **83**, 134105 (2011).

[8] S. K. Mishra, M. K. Gupta, R. Mittal, S. L. Chaplot, and T. Hansen, Appl. Phys. Lett. **101**, 242907 (2012).

[9] R. Machado, M. Sepliarsky, and M. G. Stachiotti, Phys. Rev B **84**, 134107 (2011).

[10] W. Zhong and D. Vanderbilt, Phys. Rev. Lett. **74**, 2587 (1995).

[11] O. Diéguez, K. M. Rabe, and D. Vanderbilt, Phys Rev. B **72**, 144101 (2005).

[12] W. Zhong, R. D. King-Smith, and D. Vanderbilt, Phys. Rev. Lett. **72**, 3618 (1994).

[13] R. D. King-Smith and D. Vanderbilt, Phys. Rev. B **49**, 5828 (1994).

[14] I. Tomeno, Y. Tsunoda, K. Oka, M. Matsuura, and M. Nishi, Phys. Rev. B **80**, 104101 (2009).

[15] S. J. Lin, D. P. Chiang, Y. F. Chen, C. H. Peng, H. T. Liu, J. K. Mei, W. S. Tse, T.-R. Tsai, and H.-P. Chiang, J. Raman Spectrosc. **37**, 1442 (2006).

[16] E. Bouizane, M. D. Fontana, and M. Ayadi, J. Phys.: Condens. Matter **15**, 1387 (2003).

[17] R. J. C. Lima, P. T. C. Freire, J. M. Saski, A. P. Ayala, F. E. A. Melo, J. Mendes Filho, K. C. Serra, S. Lanfredi, M. H. Lente, and J. A. Eiras, J. Raman Spectrosc. **33**, 669 (2002).

[18] Z. X. Shen, X. B. Wang, S. H. Tang, M. H. Kuok, and R. Malekfar, J. Raman Spectrosc. **31**, 439 (2000); Z. X. Shen, X. B. Wang, M. H. Kuok, and S. H. Tang, *ibid.* **29**, 379 (1998);

X. B. Wang, Z. X. Shen, Z. P. Hu, L. Qin, S. H. Tang, and M. H. Kuok, J. Mol. Struct. **385**, 1 (1996).
[19] Y. Shiratori, A. Magrez, M. Kato, K. Kasezawa, C. Pithan, and R. Waser, J. Phys. Chem. C **112**, 9610 (2008); Y. Shiratori, A. Magrez, J. Dornseiffer, F. H. Haegel, C. Pithan, and R. Waser, J. Phys. Chem. B **109**, 20122 (2005); Y. Shiratori, A. Magrez, W. Fischer, C. Pithan, and R. Waser, J. Phys. Chem. C **111**, 18493 (2007).
[20] D. L. Price and K. Skold, in *Neutron Scattering*, edited by K. Skold and D. L. Price (Academic, Orlando, 1986), Vol. A; J. M. Carpenter and D. L. Price, Phys. Rev. Lett. **54**, 441 (1985).
[21] A. Sjölander, Ark. Fys. **14**, 315 (1958).
[22] V. S. Oskotskii, Sov. Phys. Solid State **9**, 420 (1967).
[23] W. Reichardt, Primärbericht, Report No. 13.03.01p06L, 1984.
[24] P. E. Blöchl, Phys. Rev. B **50**, 17953 (1994).
[25] P. Hohenberg and W. Kohn, Phys. Rev. **136**, B864 (1964); W. Kohn and L. J. Sham, *ibid.* **140**, A1133 (1965).
[26] G. Kresse and J. Furthmüller, Comput. Mater. Sci. **6**, 15 (1996); G. Kresse and D. Joubert, Phys. Rev. B **59**, 1758 (1999).
[27] J. P. Perdew, K. Burke, and M. Ernzerhof, Phys. Rev. Lett. **77**, 3865 (1996); **78**, 1396 (1997).
[28] H. J. Monkhorst and J. D. Pack, Phys. Rev. B **13**, 5188 (1976).
[29] K. Parlinski, Z.-Q. Li, and Y. Kawazoe, Phys. Rev. Lett. **78**, 4063 (1997).
[30] K. Parlinski, software PHONON, 2010.
[31] L. Jiang, D. C. Mitchell, W. Dmowski, and T. Egami, Phys. Rev. B **88**, 014105 (2013).
[32] A. D. Bruce and R. A. Cowely, Adv. Phys. **29**, 219 (1980).
[33] N. Choudhury, E. J. Walter, A. I. Kolesnikov, and C.-K. Loong, Phys. Rev. B **77**, 134111 (2008).